

Optical+NIR analysis of a newly found Einstein ring at $z\sim 1$ from the Kilo-Degree Survey: Dark matter fraction, total and dark matter density slope and IMF

*

RUI LI ¹, NICOLA R. NAPOLITANO,^{2,3,4} GIUSEPPE D'AGO ⁵, VYACHESLAV N. SHALYAPIN,^{6,7} KAI ZHU ⁸,
XIAOTONG GUO,⁹ RAN LI,¹⁰ LÉON V. E. KOOPMANS,¹¹ CHIARA SPINIELLO,^{12,13} CRESCENZO TORTORA,¹³
FRANCESCO LA BARBERA,¹³ HAICHENG FENG,¹⁴ LIANG GAO,¹⁵ ZHIQI HUANG,¹⁶ KOEN KULJKEN,¹⁷ HUI LI,¹⁵
LINGHUA, XIE,¹⁶ MARIO RADOVICH,¹⁸ ALEXEY SERGEYEV,^{19,20,21} AND OTHERS

¹*Institute for Astrophysics, School of Physics, Zhengzhou University, Zhengzhou, 450001, China.*

²*Department of Physics “E. Pancini”, University Federico II, Via Cinthia 6, 80126-I, Naples, Italy*

³*School of Physics and Astronomy, Sun Yat-sen University, Zhuhai Campus, 2 Daxue Road, Xiangzhou District, Zhuhai, P. R. China.*

⁴*CSST Science Center for Guangdong-Hong Kong-Macau Great Bay Area, Zhuhai, 519082, P. R. China*

⁵*Institute of Astronomy, University of Cambridge, Madingley Road, Cambridge CB3 0HA, United Kingdom.*

⁶*Departamento de Física Moderna, Universidad de Cantabria, Avda. de Los Castros s/n, E-39005 Santander, Spain*

⁷*O.Ya. Usikov Institute for Radiophysics and Electronics, National Academy of Sciences of Ukraine, 12 Acad. Proscury St., UA-61085 Kharkiv, Ukraine*

⁸*Department of Astronomy, Tsinghua University, Beijing, Beijing 100084, China*

⁹*Institute of Astronomy and Astrophysics, Anqing Normal University, Anqing, Anhui 246133, China*

¹⁰*School of Physics and Astronomy, Beijing Normal University, Beijing 100875, China.*

School of Astronomy and Space Science, University of Chinese Academy of Science, Beijing 100049, China.

¹¹*Kapteyn Astronomical Institute, University of Groningen, P.O.Box 800, 9700AV Groningen, the Netherlands*

¹²*Department of Physics, University of Oxford, Denys Wilkinson Building, Keble Road, Oxford OX1 3RH, UK*

¹³*INAF – Osservatorio Astronomico di Capodimonte, Salita Moiariello 16, 80131 - Napoli, Italy*

¹⁴*Yunnan Observatories, Chinese Academy of Sciences, Kunming, 650011, Yunnan, People’s Republic of China*

¹⁵*Institute for Astrophysics, School of Physics, Zhengzhou University, Zhengzhou, 450001, China*

¹⁶*School of Physics and Astronomy, Sun Yat-sen University, Zhuhai Campus, 2 Daxue Road, Xiangzhou District, Zhuhai, P. R. China*

¹⁷*Leiden Observatory, Leiden University, P.O.Box 9513, 2300RA Leiden, The Netherlands*

¹⁸*INAF - Osservatorio Astronomico di Padova, via dell’Osservatorio 5, 35122 Padova, Italy*

¹⁹*Université Côte d’Azur, Observatoire de la Côte d’Azur, CNRS, Laboratoire Lagrange, France*

²⁰*V. N. Karazin Kharkiv National University, Kharkiv, 61022, Ukraine*

²¹*Institute of Radio Astronomy of National Academy of Science of Ukraine, Mystetstv 4, Ukraine*

ABSTRACT

We report the discovery and spectroscopic confirmation of a new bright blue Einstein ring in the Kilo Degree Survey (KiDS) footprint: the Einstein “blue eye”. Spectroscopic data from X-Shooter at the Very Large Telescope (VLT) show that the lens is a typical early-type galaxy (ETG) at $z = 0.9906$, while the background source is a Ly α emitter at $z = 2.823$. The reference lens modeling was performed on a high-resolution Y–band adaptive-optics image from HAWK-I at VLT. Assuming a singular isothermal ellipsoid (SIE) total mass density profile, we inferred an Einstein radius $R_{Ein} = 10.47 \pm 0.06$ kpc. The average slope of the total mass density inside the Einstein radius, as determined by a joint analysis of lensing and isotropic Jeans equations is $\gamma = 2.14^{+0.06}_{-0.07}$, showing no systematic deviation from the slopes of lower redshift galaxies. This can be the evidence of ETGs developing through dry mergers plus moderate dissipationless accretion. Stellar population analysis with 8-band (*grIZYJHKs*) photometries from KiDS and VIKING shows that the total stellar mass of the lens is $M_* = (3.95 \pm 0.35) \times 10^{11} M_\odot$ (Salpeter Initial Mass Function, IMF), implying a dark matter fraction inside the effective radius to be $f_{DM} = 0.307 \pm 0.151$. We finally explored the dark matter halo slope and found a strong degeneracy with the dynamic stellar mass. Dark matter adiabatic contraction is needed to explain the posterior distribution of the slope, unless IMF heavier than Salpeter is assumed.

* Based on observations with OmegaCam@VST, VIR-CAM@VISTA, HAWK-I and XSHOOTER@VLT (Prog. ID: 107.2258).

Keywords: Strong lensing — galaxies — Einstein ring

1. INTRODUCTION

Strong lensing is the effect of image distortion of far-away galaxies (sources) due to their light being bent by massive celestial bodies (lenses or deflectors), as predicted by general relativity. It is sensitive to the total mass, including dark matter (DM) and baryonic matter, and, as such, it is a crucial tool for studying the interplay between these two components (Koopmans et al. 2006, 2009; Treu & Koopmans 2004; Treu et al. 2006, 2011; Auger et al. 2009; Bolton et al. 2012; Sonnenfeld et al. 2013, 2014; He et al. 2020; Etherington et al. 2023; Li et al. 2018). With strong lensing, we can measure mass with very high precision, typically with 5% uncertainties (see e.g. Bolton et al. 2008), whereas other methods, such as galaxy dynamics and X-rays, maybe face higher uncertainties (e.g., Humphrey & Buote 2006; Napolitano et al. 2010; Tortora et al. 2022; Zhu et al. 2023). More importantly, these latter techniques become less accurate as one goes to higher redshifts (see e.g. Shetty & Cappellari 2014), where the strong lensing method is more efficient instead (see e.g. Treu & Koopmans 2004).

strong lensing has been used as a probe of the Λ CDM predictions as it offers insights into the assembly history of galaxies and their relationship with their dark matter halo centers (e.g., Fulton & Barnes 2001; Dehnen & McLaughlin 2005; Kazantzidis et al. 2006; Nipoti et al. 2009), or to probe the slope of the total mass (dark plus stellar mass) density. Statistical analyses of strong lensing systems have consistently indicated that the total mass distribution of massive early-type galaxies (ETGs) follows a power-law profile, $\rho \propto r^{-\gamma}$, with $\gamma \approx 2$ and uncertainties below 10% (Koopmans et al. 2006, 2009, Auger et al. 2009, Tortora et al. 2014, Sonnenfeld et al. 2013, Tan et al. 2023), under the assumption of isotropic velocity dispersion. This result was further confirmed by dynamics, showing an isothermal (e.g., Tortora et al. 2016) or slightly steeper (e.g. $\gamma \sim 2.2$, Bellstedt et al. 2018; Zhu et al. 2023; Li et al. 2023; Zhu et al. 2024; Wang et al. 2024) total mass density slope.

Hydrodynamical simulations have shown that $\gamma \sim 2$ is predicted at lower redshifts, where galaxy growth is driven by “dry” mergers (e.g., Nipoti et al. 2009, Remus et al. 2017). However, the redshift evolution of γ is still debated, as simulations predict the slope to become steeper ($\gamma > 2$) with increasing redshift (Remus et al. 2017, Wang et al. 2019), while some observations indicate a rather constant (Sonnenfeld et al. 2013), or decreasing γ with redshift (Bolton et al. 2012; Li et al. 2018). Unfortunately, most of these measurements are

limited to $z \lesssim 0.8$, with very few excursions to higher redshifts (MG 2016+112 at $z = 1.004$, CFRS03.1077 at $z = 0.938$; Koopmans & Treu 2002, Treu & Koopmans 2002, 2004). Hence, this poor statistics of lenses at $z \sim 1$ is a serious handicap to resolving the controversy between observations and simulations.

Another major source of systematics in the mass slope problem is the assumed stellar Initial Mass Function (IMF). This strongly impacts the stellar mass, M_* , and consequently the dark matter fraction f_{DM} of the foreground lens. Changes in the IMF normalization can increase the stellar mass-to-light ratio by more than a factor of 2, as evidenced by a large number of observations in massive elliptical galaxies (Conroy & van Dokkum 2012, Cappellari et al. 2012, La Barbera et al. 2013, Tortora et al. 2013, Spiniello et al. 2014a, Li et al. 2017, Lu et al. 2023). The choice of the IMF significantly influences conclusions regarding the DM slope. Specifically, if the IMF leads to a higher estimate of stellar mass in the galaxy center, this implies that there is less DM present. Consequently, the DM density profile must be less steep to remain consistent with the observed stellar kinematics. And vice versa for lighter IMF, which leads to lower stellar mass M_* , steeper slopes have to be assumed to replace the missing stellar masses. This can be reconciled with Λ CDM only by invoking some form of adiabatic contraction (e.g., Napolitano et al. 2010, Tortora et al. 2010, Treu et al. 2010). The degeneracy between IMF assumptions and DM slope estimates becomes particularly problematic when considering the growing evidence that the IMF may not be universal (Cappellari et al. 2012, Tortora et al. 2013, Spiniello et al. 2014b, Martín-Navarro et al. 2015, Barbosa et al. 2021, Martín-Navarro et al. 2023, Greggio & Renzini 2012). Variations in IMF with galaxy mass, stellar population properties and redshift introduce additional systematic uncertainties, as different galaxies may require distinct IMF prescriptions.

In Li et al. 2021, we identified a blue Einstein ring at $z = 0.9906$. For the peculiar appearance in the optical bands, we have dubbed it the Einstein “blue eye” (see Fig. 1). KIDSJ0233-3447 is the second most distant lens for which such a detailed analysis (e.g., velocity dispersion, stellar mass, total mass density slope, dark matter fraction and its density slope) has been performed (MG 2016+112 mentioned above being the most distant one, Koopmans & Treu 2002) and among only a limited number of confirmed lenses at $z > 0.9$ (e.g., Wong et al. 2014, Barone-Nugent et al. 2015, Cañameras et al. 2017,

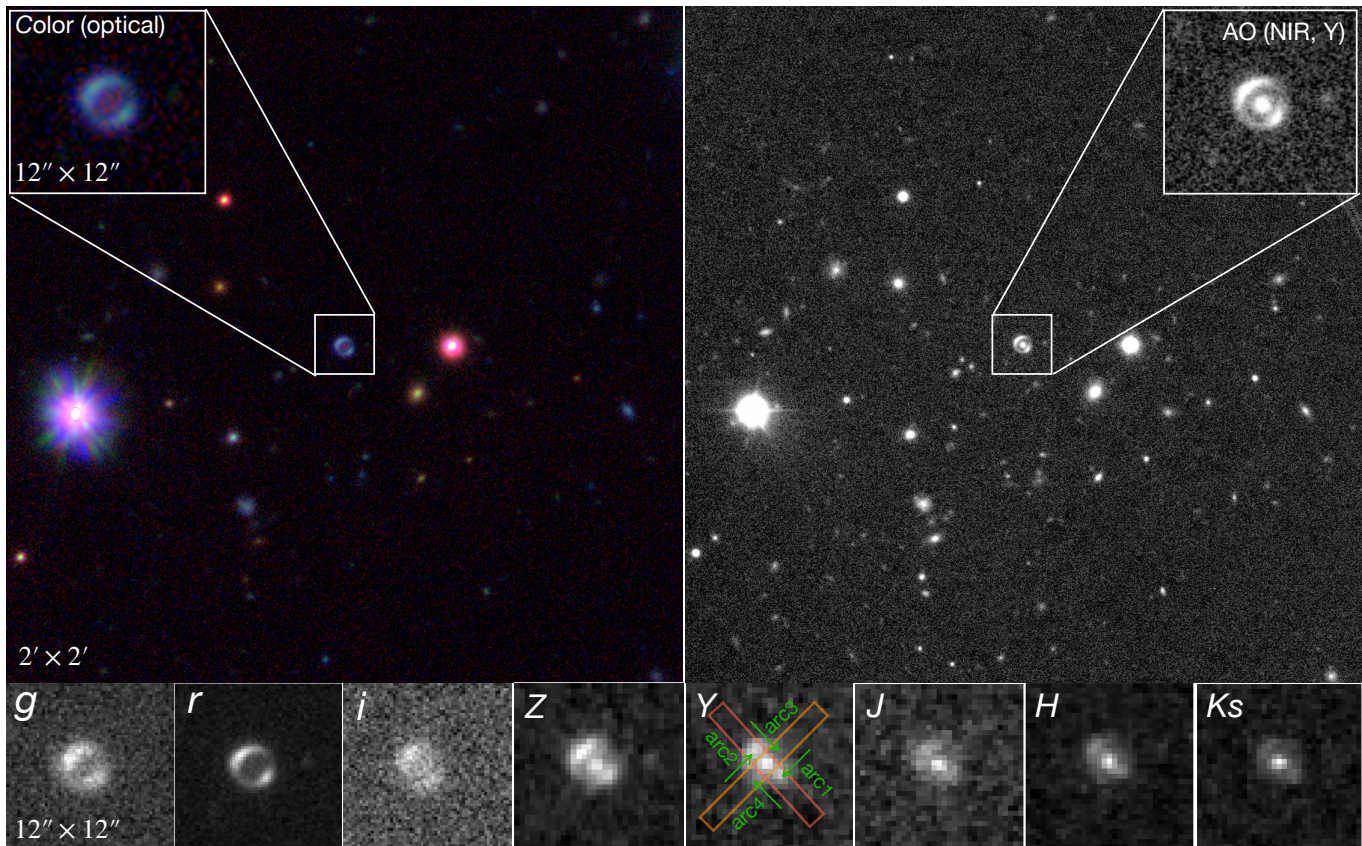


Figure 1. Images of KIDSJ0233-3447. Top left: colour-composited images ($2' \times 2'$) from KiDS observation and the zoom-in of the lens ($12'' \times 12''$). Top right: Y-band image from HAWKI@VLT ($2' \times 2'$) and the zoom-in of the lens ($12'' \times 12''$). Bottom: 8-band images from KiDS and VIKING. The two slits used for the spectroscopical observations are shown in orange (for lens) and red (for arcs) on the Y-band image. Green arrows labeled with arc 1 to arc 4 show the approximate location of the regions used to extract the spectra of the arcs (see Sec. 2.1)

Ciesla et al. 2020, van Dokkum et al. 2024), hence providing us a unique opportunity to move a step toward the understanding of the mass properties of galaxies in their early evolution phases.

In this paper, we present a comprehensive analysis of the stellar and dark matter properties of KIDSJ0233-3447 and provide a detailed discussion of IMF and the profiles of its total and dark matter mass. The paper is organized as follows: in Section 2, we introduce the data analysis. In Section 3, we provide a discussion of the results on the total mass slope, dark matter properties, and IMF model. Finally, in Section 4, we summarize our findings and draw our conclusions. For all calculations, we assume a Λ CDM cosmology with the WMAP7 (Komatsu et al. 2011) results: $(\Omega_{\Lambda}, \Omega_{\text{M}}, h) = (0.272, 0.728, 0.704)$.

2. DATA ANALYSIS AND KEY PARAMETERS

In order to perform a complete, combined and self-consistent lensing modeling, dynamics, and stellar population analysis on KIDSJ0233-3447, we have collected

seeing matched $griZYJHK_s$ photometry from the Kilo Degree Survey (KiDS, de Jong et al. 2013, Wright et al. 2024) and VISTA Kilo-degree Infrared Galaxy (VIKING, Edge et al. 2013) survey and a similarly wide wavelength baseline spectroscopy from X-Shooter, and the adaptive-optics (AO) NIR data from HAWK-I at VLT (see §2). Moreover, these data also offer the chance to assess the importance of optical + NIR datasets in strong lensing analyses, for which the KiDS+VIKING dataset is the only available precursor of optical + NIR jointing analysis of Euclid (Laureijs et al. 2011), Vera Rubin Telescope (Ivezić et al. 2019), Roman (Spergel et al. 2015) and the China Space Station Telescope (Zhan 2018).

2.1. Spectroscopic confirmation

The lens, KIDSJ0233-3447 (coordinates: 02:33:41.29 34:47:59.24), has been discovered in the Southern patch of the KiDS survey using machine learning method (Li et al. 2021). The g, r, i colour image of the system shows two bright blue arcs that form an almost perfect Einstein

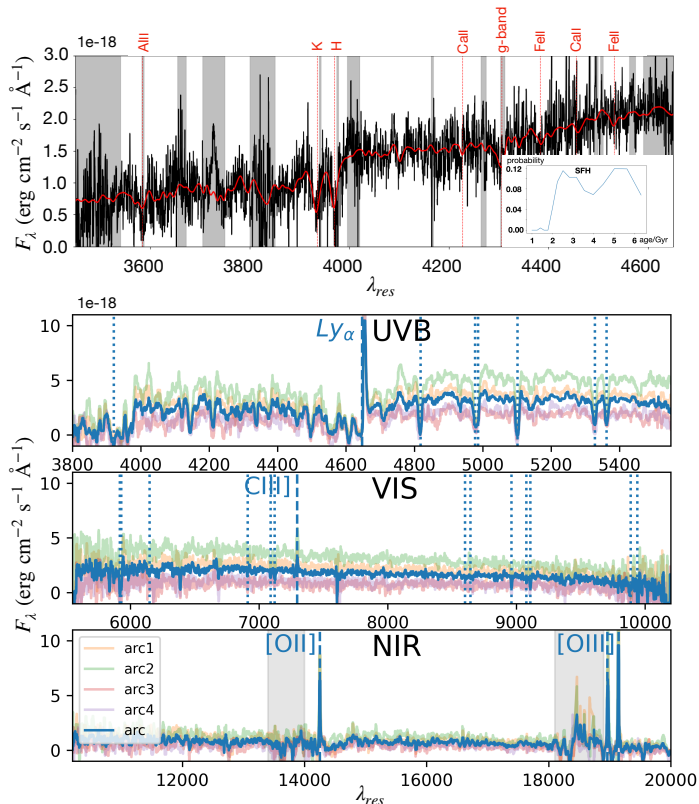


Figure 2. Top: optical arm of the spectra of the deflector (in rest-frame), obtained from X-Shooter. The 4000Å break can be seen. The velocity dispersion can be inferred from the two characteristic absorption lines, e.g. [K] and [H] bands, of elliptical galaxies. Bottom: the spectra of the lensed source in the NUV, VIS and NIR arms. The four arcs are decomposed from the two slits of different orientations (see Fig. 1). The blue (arc-ave) shows the average flux of the four arcs. The Ly α , OII, OIII lines demonstrate that the background source is a Ly α emitter at $z=2.823$.

ring (see Fig. 1). However, no central galaxy is visible in these optical observations. For the same system, the 5-band Near-Infrared (Z, Y, J, H, K_s) images from the VISTA Kilo-degree Infrared Galaxy Survey (Edge et al. 2013) show a small-sized galaxy in the center of the ring.

The optical to near-infrared spectroscopy was collected using the X-Shooter spectrograph at the VLT (ID: 107.22S8, PI: Napolitano). The observations were made in the long-slit mode, with an average seeing of approximately $0''.9$ and airmass of ~ 1.4 . The length of the slits is $11''$, and the widths for the lens are $1.3''$, $1.2''$, $1.2''$ in UVB, VIS, and NIR arms, respectively, while for the arcs are $1.3''$, $1.5''$, $1.5''$. The total integration time was 2h30m for the lens (3 exposures of 3000s each, orange slit in Fig. 1) and 1h15m for the arcs (2 exposures of 2250s each, red slit). The two different slit orientations

served to minimize the contamination of the arcs to the lens and vice versa.

Following the same method as in Spiniello et al. (2019), for the spectra observed in each slit and each arm, we decomposed the wavelength calibrated, background-subtracted and telluric-corrected 2D spectra into three components, two arcs and a central galaxy, using the accurate astrometric information provided by the strong lensing model performed on AO images (see Sec. 2.2). The VIS-arm spectrum of the central galaxy is shown in Fig. 2. We fitted the spectrum of the central galaxy with pPXF (Cappellari 2017) and found it to follow an elliptical galaxy template at $z_l = 0.9906 \pm 0.0001$, showing evident features of absorption lines of [K], [H] and G-band. We have estimated a stellar velocity dispersion inside the slit (VIS, $1.2''$ width, orange slit in Fig. 1) of 309 ± 35 km/s, using the region surrounding the prominent [K] and [H] lines. The fitting also shows a double peaks star formation history (SFH) at the age of ~ 3 Gyr and ~ 6 Gyr (see the bottom right corner in the first row). We confirmed the lensing nature of the images by comparing the four spectra decomposed in the two slits (arc1, arc2, arc3, and arc4, see, in particular, the UVB in Fig. 2), as they show a very similar continuum with the same absorption/emission lines (e.g. Ly α , CIII, [OII] and OIII emissions). Finally, we determined the source redshift from these lines in the mean spectrum of the four components and it is $z_s = 2.823 \pm 0.001$.

2.2. Lensing model with AO image

The Y-band AO images were obtained with HAWKI@VLT under the same ESO program and were reduced by the HAWK-I Pipeline¹. The final processed stacked image has a pixel scale of $0.1065''/\text{pixel}$ and point spread function (PSF) of $0.46''$ (full width at half maximum, FWHM), with a deeper exposure than those from KiDS and VIKING, making it ideal for accurate lensing modelling.

The modeling was performed using the LENSED code (Tessore et al. 2016), which allows for simultaneous modeling of the distribution of the deflector mass, and the light of the deflector, the source and the lensed images, with Markov Chain Monte Carlo (MCMC) inference. The light distribution of the lens was assumed to follow an elliptical de Vaucouleur profile (de Vaucouleurs 1948). The choice of the de Vaucouleur profile follows previous literature to be able to directly compare the results on scaling relations with SLACS (Bolton et al. 2008) and SL2S (Sonnenfeld et al. 2013) lens samples, as

¹ <https://www.eso.org/sci/facilities/paranal/instruments/hawki/doc.html>

well as with simulations (Nipoti et al. 2009). Since the source is a Ly α emitter and very little is known about the structure of these galaxies, we decided to make a more general choice and use a Sérsic profile (Sérsic 1963) for the light distribution of the source. Finally, the total mass distribution of the deflector was modeled with a singular isothermal ellipsoid (SIE, Kormann et al. 1994) profile.

In the first row of Fig. 3, we show the Y-band AO image, the best-fitting model, and the residuals obtained by LENSED. The main parameters obtained from the lens modeling are listed in Tab. 1. The Einstein radius is $R_{\text{Ein}} = 10.47 \pm 0.06$ kpc, corresponding to an Einstein mass of $M_{\text{Ein}} = 7.213 \pm 0.089 \times 10^{11} M_{\odot}$. The axis ratio for the total lensing mass is 0.932 ± 0.008 , which is a little rounder than the axis ratio of the light, $b/a = 0.85 \pm 0.08$, but consistent with this latter within the 1σ error. The effective radius of the deflector is $R_{\text{eff}} = 3.56 \pm 0.46$ kpc, about $1/3$ of R_{Ein} . These properties imply that the deflector is a massive elliptical galaxy with a round shape. The effective radius and the Sérsic index n of the source are $R_{\text{eff}} = 0.991 \pm 0.184$ kpc and $n = 1.34 \pm 0.27$, respectively, which are typical values for Ly α emitters at $z \sim 3$ (e.g., Shu et al. 2016a,b).

In order to check the robustness of the lens modeling, we have conducted an additional round of modeling and its subsequent analysis (including Sec. 2.3 and 2.4), employing a Sérsic profile for the central foreground galaxy. The parameters obtained from this analysis are also listed in Table 1. Upon comparison, it is observed that the parameters derived from the assumption of a Sérsic central galaxy are in concordance with those obtained from the de Vaucouleur model, with the exception of the effective radius R_{eff} . This discrepancy in R_{eff} subsequently influences the estimation of the total mass and the fraction of dark matter enclosed within the effective radius. Within the scope of this study, we will concentrate on the de Vaucouleur model for our foreground central galaxy assumption. Consequently, we will not delve into an in-depth discussion of the outcomes associated with the Sérsic central galaxy hypothesis.

2.3. Joint lensing and dynamical analysis

By combining the ray tracing lens modelling and the dynamics of the central galaxy, we have enough constraints to infer more detailed properties of the total mass of the lensing system, e.g. its central slope (see e.g. Treu & Koopmans 2002). For this purpose, we have assumed that the density distribution of the lens galaxy in three dimensions follows a power-law profile of

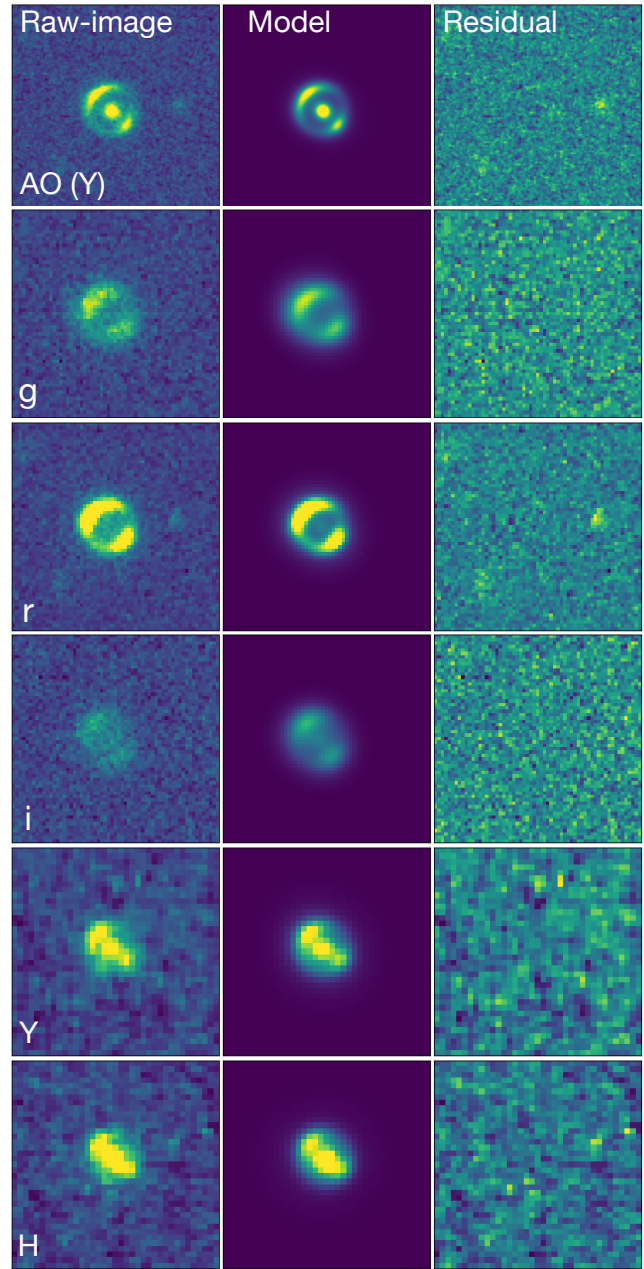


Figure 3. Multi-band strong lensing model of KIDSJ0233-3447. From top to bottom, we show the modeling of the AO (Y-band), three optical (g , r , i) and two NIR (Y, H) images. In each band, the left, middle and right panels show the observed data, the lens model and the residuals, respectively.

the form

$$\rho = \rho_0 \left(\frac{r}{r_0} \right)^{-\gamma} \quad (1)$$

where ρ_0 and r_0 , jointly, can be determined by the Einstein mass and Einstein radius, and γ denotes the logarithmic slope. We then solve the spherical Jeans equa-

Table 1. Summary of the lens main parameters

Parameters	de Vaucouleur	Sérsic
Xshooter spectroscopy		
z_1	0.9906 ± 0.0001	–
z_s	2.8230 ± 0.0001	–
σ_{slit} (km s ⁻¹)	309 ± 35	–
σ_{R_e} (km s ⁻¹)	343 ± 37	335 ± 37
Lensing model		
R_{Ein} (arcsec)	1.2926 ± 0.008	1.2899 ± 0.006
R_{Ein} (kpc)	10.47 ± 0.06	10.45 ± 0.05
lens mass b/a	0.932 ± 0.008	0.933 ± 0.007
lens mass PA	141.1 ± 3.8	141.0 ± 3.9
star mass n -index	4.0 (fixed)	5.60 ± 0.78
lens light b/a	0.85 ± 0.08	0.85 ± 0.08
lens light PA	122.6 ± 59.8	117.8 ± 58.8
lens light R_{eff} (arcsec)	0.4392 ± 0.057	0.6206 ± 0.1252
lens light R_{eff} (kpc)	3.56 ± 0.46	5.03 ± 1.01
source n -index	1.42 ± 0.26	1.34 ± 0.27
source b/a	0.76 ± 0.09	0.83 ± 0.09
source R_{eff} (arcsec)	0.123 ± 0.017	0.124 ± 0.023
source R_{eff} (kpc)	0.986 ± 0.136	0.991 ± 0.184
Dynamic and Mass estimates		
γ_{tot}	$2.195^{+0.086}_{-0.097}$	$2.202^{+0.093}_{-0.106}$
$M_{\text{Ein}}/(10^{11} M_{\odot})$	7.183 ± 0.067	7.213 ± 0.089
$M_{\text{tot}}^{\text{eff}}/(10^{11} M_{\odot})$	2.848 ± 0.369	3.805 ± 0.717
$M_*/(10^{11} M_{\odot})$ (Chab)	2.31 ± 0.20	2.06 ± 0.23
$M_*/(10^{11} M_{\odot})$ (Salp)	3.95 ± 0.35	3.71 ± 0.38
$f_{\text{DM}}(R_{\text{eff}})$ (Chab)	0.594 ± 0.088	0.729 ± 0.081
$f_{\text{DM}}(R_{\text{eff}})$ (Salp)	0.307 ± 0.151	0.512 ± 0.141

NOTE—Parameters of the lens. X-shooter spectroscopy: redshift of the lens and source and the velocity dispersion of the lens calculated in the slit and at R_{eff} . Lensing models: Einstein radius (R_{Ein}) in arcsec and kpc, followed by self-explaining parameters related to the total mass (labeled by ‘lens mass’), stellar mass parameters (labeled by ‘lens light’) and source parameters (labeled by ‘source’) light distribution. Dynamic and Mass estimates: summary of the total mass density slope (γ), mass estimates from the lensing model (M_{Ein}), and stellar population M_*^{SED} (see text for details) together with the projected DM fractions (f_{DM}).

tion (Binney & Tremaine 1987)

$$\frac{1}{\nu} \frac{d(\nu \bar{v}_r^2)}{dr} + 2 \frac{\beta \bar{v}_r^2}{r} = - \frac{GM(< r)}{r^2}, \quad (2)$$

where ν represents the density of the light particles in the galaxy, assumed to be proportional to the three-dimensional light distribution. The anisotropy parameter, β (Osipkov 1979; Merritt 1985), is set to be 0

(isotropic orbits) in our analysis, consistent with many works that analyze the velocity dispersion of massive ETGs (e.g., Koopmans et al. 2009; Auger et al. 2009). Finally, $M(< r)$ denotes the total mass contained within a sphere of radius r , corresponding to the density in Eq. 1. We performed the lensing and dynamical analyses following the method described in Li et al. (2018) (see also Koopmans et al. 2006, 2009; Bolton et al. 2012; Sonnenfeld et al. 2013). Briefly, the method consists of minimizing the χ^2 between the velocity dispersion obtained by projecting the solution of Eq. 2 within an aperture corresponding to the effective radius, and the observed one within the same aperture. At each iteration of the χ^2 , the M_{Ein} and the R_{Ein} are used to derive the ρ_0 in Eq. 1 used to solve Eq. 2. The atmospheric seeing and the aperture luminosity weighting function are also considered (see detail in Schwab et al. 2010). We found the best-fit total mass density slope to be $\gamma_{\text{tot}} = 2.14^{+0.06}_{-0.07}$. Assuming a power-law mass distribution, the total mass within the R_{eff} (consisting of both stellar and dark matter) was determined to be $M_{\text{tot}}^{\text{eff}} = (2.85 \pm 0.37) \times 10^{11} M_{\odot}$.

2.4. Stellar population from 8-band ray tracing model

We took advantage of the optical plus NIR photometry from KiDS and VIKING to derive the stellar population parameters of the lens, given that the signal-to-noise ratio of the X-shooter spectra is insufficient to perform a detailed study of the spectral indices. We have performed the lensing model on 8-bands (*griZYJHK_s*) images to derive accurate and uncontaminated multi-band magnitudes for the central galaxy. The light of the central galaxy is fitted with a de Vaucouleur profile, while the mass is assumed to be SIE. Details about the modeling can be found in appendix A. We show the model and residuals in Fig. 3 for a sample of KiDS and VIKING bands, including the Y-band to confront the AO model.

We performed the SED fitting with the multi-band photometry using the CIGALE code. For this analysis we have assumed Bruzual & Charlot (2003, BC03) stellar population templates. Parameters, such as the metallicity, extinction, star-forming rate, and age of the main stellar population were set free to vary. We used both Chabrier and Salpeter IMF, which returned a total stellar mass of $M_{\text{SED}}^{\text{Chab}} = (2.31 \pm 0.20) \times 10^{11} M_{\odot}$, and $M_{\text{SED}}^{\text{Salp}} = (3.95 \pm 0.35) \times 10^{11} M_{\odot}$, respectively. Given $R_{\text{eff}} = 3.56 \pm 0.46$ kpc, we found that the mass-size relation of this galaxy is fully consistent with ETGs at redshift $z \sim 1$ (see Sonnenfeld et al. 2013). Finally, by subtracting the stellar mass from the total mass, we obtained the DM mass, and then the DM fraction inside the effective radius, which are $f_{\text{DM}}^{\text{Chab}} = 0.594 \pm 0.088$ for

the Chabrier and $f_{DM}^{\text{Salp}} = 0.307 \pm 0.151$ for the Salpeter IMF.

The stellar population analysis returned a galaxy age of 5.9 (Chabrier IMF) or 5.6 Gyrs (Salpeter IMF), suggesting an old stellar population and an early formation epoch but with a rather extended delayed star formation history $\text{SFH} \propto t/\tau^2 \exp(-t/\tau)$, with a $\tau \sim 0.8$ Gyr. The old age has been confirmed by the PPXF analysis of the X-Shooter spectra showing a double-peaked SFH, at ~ 5.5 Gyr and ~ 2.5 Gyr in lookback time (see the top panel in Fig. 2), hence fully compatible with old age and an extended SFH. This is a much older age than the one found from another high- z lens, MG 2016+112 which shows younger stellar populations (Treu & Koopmans 2002).

3. DISCUSSION ON THE PROPERTIES

3.1. Total mass density slope and dark matter fraction

As mentioned above, the lensing galaxy KiDSJ0233-3447 is the second galaxy at $z \sim 1$ for which a total density slope measurement has been obtained after MG2016+112. The latter system has many similarities with KiDSJ0233-3447, such as a foreground redshift of $z = 1.044$, source redshift of $z = 3.263$ and a velocity dispersion of 304 ± 27 km/s inside the effective radius. The density slopes of KiDSJ0233-3447 ($\gamma_{tot} = 2.14^{+0.06}_{-0.07}$) and MG 2016+112 ($\gamma_{tot} = 2.0 \pm 0.1$) are also consistent within 1σ , but the Einstein “blue eye” slope is consistent with an isothermal distribution ($\rho \propto r^{-2}$) only at 2σ -level.

Ruff et al. (2011) and Bolton et al. (2012) claimed that the total mass density slope γ_{tot} should increase with cosmic time. However, this appears inconsistent with simulations of dry merger-driven evolution in ETGs. Nipoti et al. (2009) suggested that dry mergers might preserve the nearly isothermal structure of galaxies during $0 < z < 1$. Later analyses by Sonnenfeld et al. (2014) demonstrate that pure dry mergers predict a substantial decrease in density slope over time, conflicting with lensing observations indicating either increasing or constant γ_{tot} . When incorporating modest dissipative processes (e.g., gas accretion), the central density profile can steepen, offsetting the flattening effects of dry mergers. This mechanism enables γ_{tot} to remain constant from $z \sim 1$ to $z=0$.

Given the scarcity of gas in ETGs to allow wet mergers, the only viable reconciliation between observations and simulations requires non-evolution of γ_{tot} with redshift. SL2S lenses ($0 \lesssim z \lesssim 0.8$) measured $\gamma_{tot} = 2.05 \pm 0.06$ (Sonnenfeld et al. 2013). While SLACS samples previously suggested slightly steeper slopes ($\gamma_{tot} = 2.078 \pm 0.027$), recent work by Sonnen-

feld (2024) reveals these measurements may be overestimated by ~ 0.1 due to selection biases. Lenses at $z \sim 1$ like KiDS0233-3447 and MG 2016+112 exhibit slopes comparable to these lower-redshift lenses. We therefore suggest that the “blue eye” shows no systematic deviation from low-redshift slopes, supporting slope stability at $z < 1$ (e.g., Koopmans et al. 2006; Sonnenfeld et al. 2013). This evidence suggests ETG evolution through combined dry mergers and moderate dissipationless accretion. Such hybrid evolution simultaneously explains observed size growth and γ_{tot} stability.

However, the total density slope γ_{tot} is a combination of 1) the shallower (typically ~ 1) dark matter and the steeper (typically ~ 3) stellar matter slopes (see e.g. Graham et al. 2006) in the galaxy centers and 2) their relative mass fraction. A larger DM fraction generally leads to a shallower total density profile, closer to the DM slope, while a lower DM fraction would produce a slope more biased toward the steeper starlight. Interestingly, when DM and stars almost balance, the slope conspires toward an isothermal value, $\gamma_{tot} \sim 2$. Lens systems, indeed show a variety of slopes and a correlation with f_{DM} that follows this intuitive picture, as it can be seen in the left panel of Fig. 4. Here, we show the correlation between the density slope γ_{tot} and the dark matter fraction f_{DM}^{Salp} for the SL2S sample from Sonnenfeld et al. (2013). We have chosen the SL2S sample for uniformity on the model assumptions, as they provide the f_{DM} inside the effective radius R_{eff} , like us, and unlike SLACS (Auger et al. 2009), using half R_{eff} . Also, SL2S employs multi-band photometry to calculate the stellar mass, although they have a narrower wavelength baseline than ours. Finally, the SL2S sample covers a wider redshift range than the SLACS, with the highest- z lens at $z \sim 0.781$, closer to the redshift of the Einstein “blue eye”. Finally we use the de Vaucouleur profile as in SL2S.

In Fig. 4, KiDSJ0233-3447 shows a $\gamma_{tot} = 2.14^{+0.06}_{-0.07}$, which is fully consistent with the correlation from the SL2S sample. In the same figure, we also show that the situation is different if we assume a Sérsic model for the foreground galaxy instead of a de Vaucouleur (full lensing parameters reported in Table 1), mainly due to the larger R_{eff} . We might expect that a similar correction toward larger DM fraction could apply to the SL2S sample if a Sérsic model were adopted but, overall, the conclusion about the consistent trend between f_{DM} and γ would remain unchanged, not certainly worsened.

Here we note that the observed $\gamma_{tot} - f_{DM}$ relation in the SL2S sample, as well as in other lensing samples (e.g., SLACS; Shajib et al. 2021), exhibits discrepancies with cosmological simulations. Hydrodynamical simu-

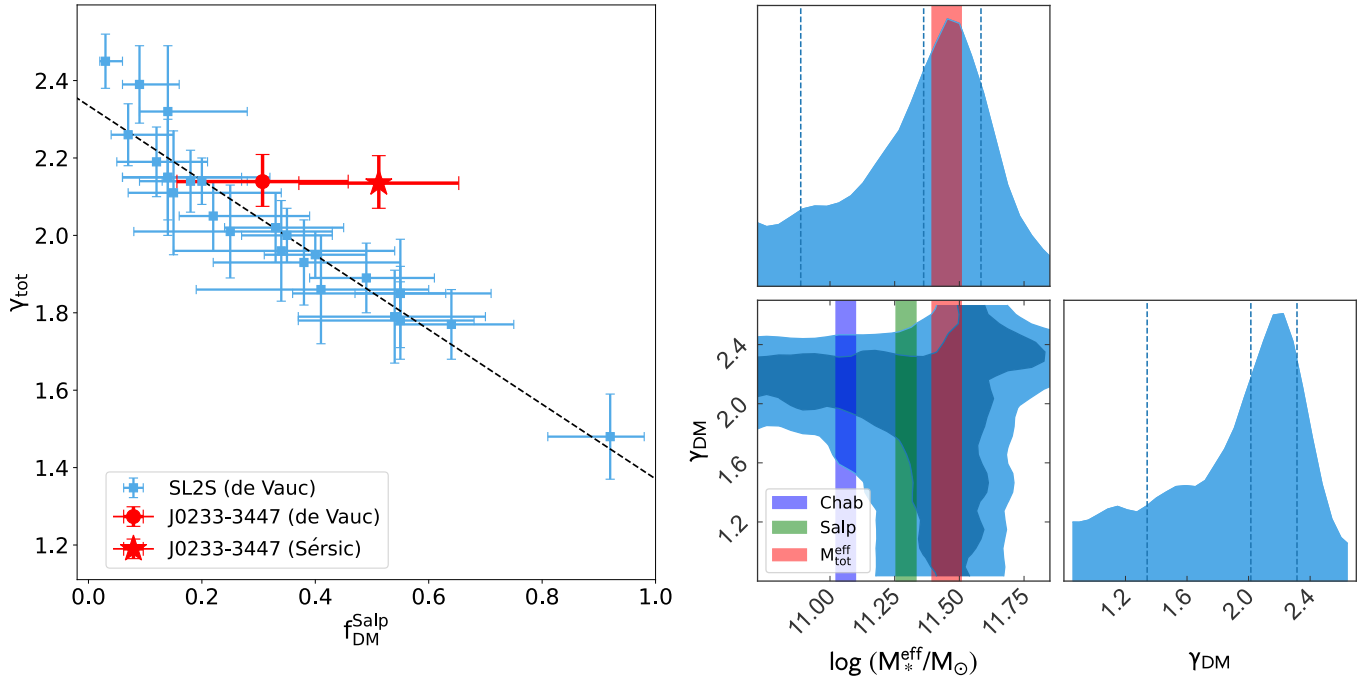


Figure 4. Left: The relationship between total mass density slope γ_{tot} and dark matter fraction (Salpeter IMF, f_{DM}^{Salp}) for SL2S sample (squares) and of KiDSJ0233-3447 by assuming de Vaucouleur (dot) and Sérsic (star) foreground light profile. The black dashed line shows the line fit of the SL2S sample. Right: The MCMC inference for dark matter slope γ_{DM} and stellar mass. The stellar mass inferred from Chabrier and Salpeter IMF are shown with blue and green bars, respectively.

lations either reproduce the γ_{tot} distribution but systematically underestimate f_{DM} when baryonic physics is minimally included (e.g., Duffy et al. 2010; Johansson et al. 2012), or recover the observed f_{DM} with strong feedback at the expense of predicting shallower slopes than observed (e.g., Dubois et al. 2013; Xu et al. 2017). The $\gamma_{tot} - f_{DM}$ relation of KIDSJ0233-3447 aligns with previous lensing studies at lower redshifts (e.g., Shajib et al. 2021), indicating the tension with simulations is also exists at higher redshift ($z \sim 1$). This persistent mismatch highlights the need for either refined implementations of feedback mechanisms in cosmological simulations or a critical re-examination of potential systematic biases in observational analyses.

3.2. IMF and dark matter slope

The analysis presented in Section 3.1 adopts the Salpeter IMF as a wavelength baseline for comparison, aligning with the approach utilized in the SL2S study. It is acknowledged, however, that the IMF is not necessarily confined to the Salpeter IMF, with evidence suggesting variations in the IMF across different galaxies. The choice of IMF influences the estimation of the dark matter fraction, which, in turn, has implications for the measurement of the dark matter density slope. Specifically, the possibility that KiDSJ0233-3447 favors a lighter or a heavier IMF, for a fixed total slope, has di-

rect consequences on the inferred DM halo density slope. For instance, a higher DM fraction given from a lighter IMF would imply an excess of DM which might not be compatible with some standard Λ CDM halo. Hence, we need to evaluate how much the DM slope can vary in response to some physically motivated IMF variation. To check this, we have combined lensing and dynamics again. But instead of a single power-law, we consider the total mass of the galaxy in Eq. 2 made of the stellar and the dark matter components, and then use Bayesian inference to obtain the posterior distribution of dynamical stellar mass and dark matter slope. The stellar mass is assumed to follow the de Vaucouleur profile, as in Table 1, with a dynamical mass-to-light ratio as a free parameter ($M_*^{dyn}(r) = M/L_*^{dyn} \times L_{tot}^{deV}(r)$, being the $L_{tot}^{deV}(r)$ the growth curve of the deprojected de Vaucouleur profile). For the dark matter, we assume a power-law distribution with slope γ_{DM} , which is the second free parameter in the Bayesian inference. We note that the stellar mass obtained here is dynamically inferred and we can use its ratio with the SED/IMF inferred stellar masses, as a proxy of the variation of the IMF.

In Fig. 4, we report the confidence contours (68% and 95%) and the marginalized posterior probabilities (16%, 50% and 84%, from left to right vertical dashed lines) of the two parameters in our model. To have a

more physical insight of the inferences, on the x-axis we report the stellar mass inside the R_{eff} corresponding to the inferred M/L_*^{dyn} as this can be compared with the inferences of the SED/IMFs (namely Chabrier and Salpeter IMF) and with the total mass inside the same radius from the lensing + dynamics, all marked as vertical stripes in the figure. This latter, in particular, fixes the upper limit the stellar mass can be reasonably expected to reach, under the “unphysical” condition of no dark matter inside R_{eff} .

From the confidence contours, we see a degeneracy between M_*^{eff} and γ_{DM} . IMF normalizations above a Salpeter IMF are compatible with a larger variety of DM slope, between $\gamma_{DM} \sim 2.3$ and down to $\gamma_{DM} \sim 1$. However, using the $M_{\text{tot}}^{\text{eff}}$ as a physical upper limit for the stellar mass, we see that the accessible parameter space at low γ_{DM} is strongly restricted. A reasonable solution for an IMF steeper than the Salpeter IMF should have a stellar mass $\log M_*^{\text{eff}} = 11.36 \pm 0.05$ (i.e. around the lower limit of $M_{\text{tot}}^{\text{eff}}$) and a $\gamma_{DM} \sim 1.6 \pm 0.6$, which would correspond to a $f_{DM} = 0.20$, perfectly reconciling the “blue eye” with the SL2S sample (see §3.1). This case is statistically consistent with a standard NFW profile.

On the other hand, if one wants to stick to a Salpeter IMF, the $\log M_*^{\text{eff}} = 11.30 \pm 0.04$ and a $\gamma_{DM} \sim 2.0 \pm 0.4$, which would correspond to a $f_{DM} = 0.31$ (see also the lensing+dynamics analysis presented in §3.1). Considering that the DM slope is estimated within the R_{eff} , we can follow Napolitano et al. (2010) (see also Graham et al. 2006) and assume a dilution of the dark matter slope of $\Delta\gamma_{DM} \sim 0.3$ with respect to the true central cusp, to find that this case is clearly steeper than a NFW ($\gamma_{DM}^{\text{true}} = 2.0 - 0.4 > 1.0 \pm 0.3$) and more compatible with a contracted halo. A similar conclusion was also reached by Sonnenfeld et al. (2012), where they analyzed a double Einstein ring lens at a low redshift ($z = 0.222$) and inferred a dark matter slope of $\gamma_{DM} = 1.7 \pm 0.2$ and Napolitano et al. (2010) who found $\gamma_{DM} \sim 1.6$ for a sample of local galaxies. Such a co-existence of Salpeter IMF and dark matter halo contraction has also been found in other works (e.g., Treu et al. 2010; Tortora et al. 2010; Spiniello et al. 2011; Sonnenfeld et al. 2013), suggesting it can be a regular feature in massive elliptical systems (but see Mendel et al. 2020).

Finally, according to the posterior probability, we cannot rule out the possibility of a lighter IMF than the Salpeter IMF, which would not alter the overall DM slope, yet compatible with a contracted halo. In particular, we see that a Chabrier or even lighter IMF is compatible with a steep DM slope up to $\gamma_{DM} \gtrsim 2.0$, which is strongly deviating from the Λ CDM DM-only simulation predictions (i.e. a NFW profile, Navarro et al. 1997).

The main implication of such an IMF would be an increased dark matter fraction of $f_{DM} \sim 0.6$ (see Tab. 1). Such a DM fraction is larger than typical values found in observations for lower redshift galaxies (e.g. COMA, Thomas et al. 2007; SLACS ($f_{DM} < 0.6$ Barnabè et al. 2011), and almost twice that expected from simulations for a Chabrier IMF at $z \sim 1$ (Oser et al. 2010; Remus et al. 2017).

Although the arguments discussed above support both the Salpeter and Chabrier IMFs with a contracted halo, we can provide more direct evidence to support that KiDSJ0233-3447 favors a heavier IMF (e.g., Salpeter) combined with contraction over a standard uncontracted NFW profile. Indeed, in a heavy halo contraction, one expects the dissipation of cold gas to play a strong role (see e.g. Gnedin et al. 2004; Sellwood & McGaugh 2005). According to the inferred SFH, both from the multiband photometry and the X-Shooter spectrum, the “blue eye” central galaxy has gone through a quite long and massive star-formation activity, which lasted for ~ 6 Gyr and ended just before $z \sim 1$. In particular, the double-peaked SFH suggested by PPXF might even suggest a major accretion event. We argue that this extended SFH might have favored the halo contraction of the central galaxy. We remark here that an extended (even double-peaked) SFH is consistent with the two-stage formation model proposed by Weidner et al. (2013) that can explain both a bottom-heavy IMF and a solar metallicity observed in high- z ETGs. According to this model, galaxies have formed $\sim 10\%$ of their stars during a very short burst, lasting 0.3 Gyr, with a top-heavy IMF, then followed by a second stage where the bulk of the stellar mass is formed in about 1 Gyr, with a bottom-heavy IMF. If so, the “blue eye” central galaxy can be a test bench of this model, showing eventually even a more prolonged process, possibly driven by the higher velocity dispersion (and hence mass) of KiDSJ0233-3447, with respect to the typical galaxies considered in Weidner et al. (2013).

4. CONCLUSION

We have provided the first full optical + NIR photometric and spectroscopic analysis of an Einstein ring at $z \sim 1$. KiDSJ0233-3447 is a new strong lens discovered in KiDS, which we followed up with the X-shooter and HAWKI instruments at the VLT. The foreground galaxy is an early-type galaxy (ETG) located at $z = 0.9906$, while the background source is a Ly α emitter at $z = 2.832$.

We collected a combined multi-band (optical to infrared), AO, and spectroscopic dataset for this lens, which allowed us to perform a complete multi-band

analysis of the system, including an 8-band lens model. With the analysis, we can constrain The lens parameters in the 8-band models with excellent accuracy, despite the different seeing conditions and image quality of the cameras adopted. The Einstein radius and effective radius are 10.47 ± 0.06 kpc and 3.56 ± 0.46 kpc, respectively and the total mass density slope (obtained via lensing-dynamical analysis) is $2.139_{-0.070}^{+0.064}$, which is close to the isothermal density profile, consistent with previous lower-redshift strong lenses. This supports a scenario of dry merger plus modest dissipative processes (such as gas accretion) driving the ETGs evolution between $0 < z < 1$ (Sonnenfeld et al. 2014).

We reported a dark matter fraction within R_{eff} to be $f_{DM} = 0.307 \pm 0.151$ (assuming a Salpeter IMF), which is consistent with values typically observed in strong lensing systems at lower redshifts and similar masses. To explore whether this dark matter fraction could result from an unaccounted heavier IMF, we found that such a scenario would imply a standard NFW halo (i.e., $\gamma_{DM=1}$) with $f_{DM} \sim 0.20$. On the other hand, if we assume a Salpeter IMF, the observed dark matter fraction would suggest a contracted halo with a dark matter slope of $\gamma_{DM} > 1.6$, consistent with other evidence from low-redshift galaxies.

The old age (~ 6 Gyr) and the extended star formation history derived by both the 8-band photometry from the ray-tracing and the X-Shooter of the central spectrum, support the contraction + Salpeter IMF. In particular, the Einstein “blue eye” provides evidence of

the two-stage IMF scenario (Weidner et al. 2013) for early-stage of ETG formation.

Finally, KiDSJ0233-3447 represents a reference case for analyses that will combine similar wide wavelength baseline datasets, from optical to NIR, from future surveys from ground and from space.

ACKNOWLEDGEMENTS

Rui Li acknowledges the National Nature Science Foundation of China (No. 12203050) and the Natural Science Foundation of Henan Province of China (Grant No.242300420235). NRN acknowledges financial support from the Research Fund for International Scholars of the National Science Foundation of China, grant n. 12150710511. Ran Li acknowledges the support of National Nature Science Foundation of China (Nos 11988101), the support by National Key R&D Program of China No. 2022YFF0503403, the support from the Ministry of Science and Technology of China (Nos. 2020SKA0110100), the science research grants from the China Manned Space Project, CAS Project for Young Scientists in Basic Research (No. YSBR-062), and the support from K.C.Wong Education Foundation. CT acknowledges funding from INAF research grant 2022 LEMON. HCF acknowledge the financial support of the National Natural Science Foundation of China (grant No. 12203096) and Yunnan Fundamental Research Projects (grant No. 202301AT070339). GD acknowledges support by UKRI-STFC grants: ST/T003081/1 and ST/X001857/1

REFERENCES

- Auger, M. W., Treu, T., Bolton, A. S., et al. 2009, *ApJ*, 705, 1099, doi: [10.1088/0004-637X/705/2/1099](https://doi.org/10.1088/0004-637X/705/2/1099)
- Barbosa, C. E., Spiniello, C., Arnaboldi, M., et al. 2021, *A&A*, 645, L1, doi: [10.1051/0004-6361/202039810](https://doi.org/10.1051/0004-6361/202039810)
- Barnabè, M., Czoske, O., Koopmans, L. V. E., Treu, T., & Bolton, A. S. 2011, *MNRAS*, 415, 2215, doi: [10.1111/j.1365-2966.2011.18842.x](https://doi.org/10.1111/j.1365-2966.2011.18842.x)
- Barone-Nugent, R. L., Sonnenfeld, A., Wyithe, J. S. B., et al. 2015, *MNRAS*, 453, 3068, doi: [10.1093/mnras/stv1872](https://doi.org/10.1093/mnras/stv1872)
- Bellstedt, S., Forbes, D. A., Romanowsky, A. J., et al. 2018, *MNRAS*, 476, 4543, doi: [10.1093/mnras/sty456](https://doi.org/10.1093/mnras/sty456)
- Binney, J., & Tremaine, S. 1987, *Galactic dynamics*
- Bolton, A. S., Burles, S., Koopmans, L. V. E., et al. 2008, *ApJ*, 682, 964, doi: [10.1086/589327](https://doi.org/10.1086/589327)
- Bolton, A. S., Brownstein, J. R., Kochanek, C. S., et al. 2012, *ApJ*, 757, 82, doi: [10.1088/0004-637X/757/1/82](https://doi.org/10.1088/0004-637X/757/1/82)
- Bruzual, G., & Charlot, S. 2003, *MNRAS*, 344, 1000, doi: [10.1046/j.1365-8711.2003.06897.x](https://doi.org/10.1046/j.1365-8711.2003.06897.x)
- Cañameras, R., Nesvadba, N. P. H., Kneissl, R., et al. 2017, *A&A*, 600, L3, doi: [10.1051/0004-6361/201630359](https://doi.org/10.1051/0004-6361/201630359)
- Cappellari, M. 2017, *MNRAS*, 466, 798, doi: [10.1093/mnras/stw3020](https://doi.org/10.1093/mnras/stw3020)
- Cappellari, M., McDermid, R. M., Alatalo, K., et al. 2012, *Nature*, 484, 485, doi: [10.1038/nature10972](https://doi.org/10.1038/nature10972)
- Ciesla, L., Béthermin, M., Daddi, E., et al. 2020, *A&A*, 635, A27, doi: [10.1051/0004-6361/201936727](https://doi.org/10.1051/0004-6361/201936727)
- Conroy, C., & van Dokkum, P. G. 2012, *ApJ*, 760, 71, doi: [10.1088/0004-637X/760/1/71](https://doi.org/10.1088/0004-637X/760/1/71)
- de Jong, J. T. A., Verdoes Kleijn, G. A., Kuijken, K. H., & Valentijn, E. A. 2013, *Experimental Astronomy*, 35, 25, doi: [10.1007/s10686-012-9306-1](https://doi.org/10.1007/s10686-012-9306-1)
- de Vaucouleurs, G. 1948, *Annales d’Astrophysique*, 11, 247
- Dehnen, W., & McLaughlin, D. E. 2005, *MNRAS*, 363, 1057, doi: [10.1111/j.1365-2966.2005.09510.x](https://doi.org/10.1111/j.1365-2966.2005.09510.x)

- Dubois, Y., Gavazzi, R., Peirani, S., & Silk, J. 2013, MNRAS, 433, 3297, doi: [10.1093/mnras/stt997](https://doi.org/10.1093/mnras/stt997)
- Duffy, A. R., Schaye, J., Kay, S. T., et al. 2010, MNRAS, 405, 2161, doi: [10.1111/j.1365-2966.2010.16613.x](https://doi.org/10.1111/j.1365-2966.2010.16613.x)
- Edge, A., Sutherland, W., Kuijken, K., et al. 2013, The Messenger, 154, 32
- Etherington, A., Nightingale, J. W., Massey, R., et al. 2023, MNRAS, 521, 6005, doi: [10.1093/mnras/stad582](https://doi.org/10.1093/mnras/stad582)
- Fulton, E., & Barnes, J. E. 2001, Ap&SS, 276, 851, doi: [10.1023/A:1017560704291](https://doi.org/10.1023/A:1017560704291)
- Gnedin, O. Y., Kravtsov, A. V., Klypin, A. A., & Nagai, D. 2004, ApJ, 616, 16, doi: [10.1086/424914](https://doi.org/10.1086/424914)
- Graham, A. W., Merritt, D., Moore, B., Diemand, J., & Terzić, B. 2006, AJ, 132, 2701, doi: [10.1086/508990](https://doi.org/10.1086/508990)
- Greggio, L., & Renzini, A. 2012, arXiv e-prints, arXiv:1203.1221, doi: [10.48550/arXiv.1203.1221](https://doi.org/10.48550/arXiv.1203.1221)
- He, Q., Li, H., Li, R., et al. 2020, MNRAS, 496, 4717, doi: [10.1093/mnras/staa1769](https://doi.org/10.1093/mnras/staa1769)
- Humphrey, P. J., & Buote, D. A. 2006, ApJ, 639, 136, doi: [10.1086/499323](https://doi.org/10.1086/499323)
- Ivezić, Ž., Kahn, S. M., Tyson, J. A., et al. 2019, ApJ, 873, 111, doi: [10.3847/1538-4357/ab042c](https://doi.org/10.3847/1538-4357/ab042c)
- Johansson, P. H., Naab, T., & Ostriker, J. P. 2012, ApJ, 754, 115, doi: [10.1088/0004-637X/754/2/115](https://doi.org/10.1088/0004-637X/754/2/115)
- Kazantzidis, S., Zentner, A. R., & Kravtsov, A. V. 2006, ApJ, 641, 647, doi: [10.1086/500579](https://doi.org/10.1086/500579)
- Komatsu, E., Smith, K. M., Dunkley, J., et al. 2011, ApJS, 192, 18, doi: [10.1088/0067-0049/192/2/18](https://doi.org/10.1088/0067-0049/192/2/18)
- Koopmans, L. V. E., & Treu, T. 2002, ApJL, 568, L5, doi: [10.1086/340143](https://doi.org/10.1086/340143)
- Koopmans, L. V. E., Treu, T., Bolton, A. S., Burles, S., & Moustakas, L. A. 2006, ApJ, 649, 599, doi: [10.1086/505696](https://doi.org/10.1086/505696)
- Koopmans, L. V. E., Bolton, A., Treu, T., et al. 2009, ApJL, 703, L51, doi: [10.1088/0004-637X/703/1/L51](https://doi.org/10.1088/0004-637X/703/1/L51)
- Kormann, R., Schneider, P., & Bartelmann, M. 1994, A&A, 284, 285
- La Barbera, F., Ferreras, I., Vazdekis, A., et al. 2013, MNRAS, 433, 3017, doi: [10.1093/mnras/stt943](https://doi.org/10.1093/mnras/stt943)
- Laureijs, R., Amiaux, J., Arduini, S., et al. 2011, arXiv e-prints, arXiv:1110.3193, <https://arxiv.org/abs/1110.3193>
- Li, H., Ge, J., Mao, S., et al. 2017, ApJ, 838, 77, doi: [10.3847/1538-4357/aa662a](https://doi.org/10.3847/1538-4357/aa662a)
- Li, R., Shu, Y., & Wang, J. 2018, MNRAS, 480, 431, doi: [10.1093/mnras/sty1813](https://doi.org/10.1093/mnras/sty1813)
- Li, R., Napolitano, N. R., Spiniello, C., et al. 2021, ApJ, 923, 16, doi: [10.3847/1538-4357/ac2df0](https://doi.org/10.3847/1538-4357/ac2df0)
- Li, S., Li, R., Zhu, K., et al. 2023, arXiv e-prints, arXiv:2310.13278, doi: [10.48550/arXiv.2310.13278](https://doi.org/10.48550/arXiv.2310.13278)
- Lu, S., Zhu, K., Cappellari, M., et al. 2023, arXiv e-prints, arXiv:2309.12395, doi: [10.48550/arXiv.2309.12395](https://doi.org/10.48550/arXiv.2309.12395)
- Martín-Navarro, I., Vazdekis, A., La Barbera, F., et al. 2015, ApJL, 806, L31, doi: [10.1088/2041-8205/806/2/L31](https://doi.org/10.1088/2041-8205/806/2/L31)
- Martín-Navarro, I., de Lorenzo-Cáceres, A., Gadotti, D. A., et al. 2023, arXiv e-prints, arXiv:2312.13355, doi: [10.48550/arXiv.2312.13355](https://doi.org/10.48550/arXiv.2312.13355)
- Mendel, J. T., Beifiori, A., Saglia, R. P., et al. 2020, ApJ, 899, 87, doi: [10.3847/1538-4357/ab9ffc](https://doi.org/10.3847/1538-4357/ab9ffc)
- Merritt, D. 1985, AJ, 90, 1027, doi: [10.1086/113810](https://doi.org/10.1086/113810)
- Napolitano, N. R., Romanowsky, A. J., & Tortora, C. 2010, MNRAS, 405, 2351, doi: [10.1111/j.1365-2966.2010.16710.x](https://doi.org/10.1111/j.1365-2966.2010.16710.x)
- Navarro, J. F., Frenk, C. S., & White, S. D. M. 1997, ApJ, 490, 493, doi: [10.1086/304888](https://doi.org/10.1086/304888)
- Nipoti, C., Treu, T., & Bolton, A. S. 2009, ApJ, 703, 1531, doi: [10.1088/0004-637X/703/2/1531](https://doi.org/10.1088/0004-637X/703/2/1531)
- Oser, L., Ostriker, J. P., Naab, T., Johansson, P. H., & Burkert, A. 2010, ApJ, 725, 2312, doi: [10.1088/0004-637X/725/2/2312](https://doi.org/10.1088/0004-637X/725/2/2312)
- Osipkov, L. P. 1979, Pisma v Astronomicheskii Zhurnal, 5, 77
- Remus, R.-S., Dolag, K., Naab, T., et al. 2017, MNRAS, 464, 3742, doi: [10.1093/mnras/stw2594](https://doi.org/10.1093/mnras/stw2594)
- Ruff, A. J., Gavazzi, R., Marshall, P. J., et al. 2011, ApJ, 727, 96, doi: [10.1088/0004-637X/727/2/96](https://doi.org/10.1088/0004-637X/727/2/96)
- Schwab, J., Bolton, A. S., & Rappaport, S. A. 2010, ApJ, 708, 750, doi: [10.1088/0004-637X/708/1/750](https://doi.org/10.1088/0004-637X/708/1/750)
- Sellwood, J. A., & McGaugh, S. S. 2005, ApJ, 634, 70, doi: [10.1086/491731](https://doi.org/10.1086/491731)
- Sérsic, J. L. 1963, Boletín de la Asociación Argentina de Astronomía La Plata Argentina, 6, 41
- Shajib, A. J., Treu, T., Birrer, S., & Sonnenfeld, A. 2021, MNRAS, 503, 2380, doi: [10.1093/mnras/stab536](https://doi.org/10.1093/mnras/stab536)
- Shetty, S., & Cappellari, M. 2014, ApJL, 786, L10, doi: [10.1088/2041-8205/786/2/L10](https://doi.org/10.1088/2041-8205/786/2/L10)
- Shu, Y., Bolton, A. S., Kochanek, C. S., et al. 2016a, ApJ, 824, 86, doi: [10.3847/0004-637X/824/2/86](https://doi.org/10.3847/0004-637X/824/2/86)
- Shu, Y., Bolton, A. S., Mao, S., et al. 2016b, ApJ, 833, 264, doi: [10.3847/1538-4357/833/2/264](https://doi.org/10.3847/1538-4357/833/2/264)
- Sonnenfeld, A. 2024, A&A, 690, A325, doi: [10.1051/0004-6361/202451341](https://doi.org/10.1051/0004-6361/202451341)
- Sonnenfeld, A., Nipoti, C., & Treu, T. 2014, ApJ, 786, 89, doi: [10.1088/0004-637X/786/2/89](https://doi.org/10.1088/0004-637X/786/2/89)
- Sonnenfeld, A., Treu, T., Gavazzi, R., et al. 2012, ApJ, 752, 163, doi: [10.1088/0004-637X/752/2/163](https://doi.org/10.1088/0004-637X/752/2/163)
- . 2013, ApJ, 777, 98, doi: [10.1088/0004-637X/777/2/98](https://doi.org/10.1088/0004-637X/777/2/98)
- Spergel, D., Gehrels, N., Baltay, C., et al. 2015, arXiv e-prints, arXiv:1503.03757, doi: [10.48550/arXiv.1503.03757](https://doi.org/10.48550/arXiv.1503.03757)

- Spiniello, C., Koopmans, L. V. E., Trager, S. C., Czoske, O., & Treu, T. 2011, *MNRAS*, 417, 3000, doi: [10.1111/j.1365-2966.2011.19458.x](https://doi.org/10.1111/j.1365-2966.2011.19458.x)
- Spiniello, C., Trager, S., Koopmans, L. V. E., & Conroy, C. 2014a, *MNRAS*, 438, 1483, doi: [10.1093/mnras/stt2282](https://doi.org/10.1093/mnras/stt2282)
- . 2014b, *MNRAS*, 438, 1483, doi: [10.1093/mnras/stt2282](https://doi.org/10.1093/mnras/stt2282)
- Spiniello, C., Sergeev, A. V., Marchetti, L., et al. 2019, *MNRAS*, 485, 5086, doi: [10.1093/mnras/stz781](https://doi.org/10.1093/mnras/stz781)
- Tan, C. Y., Shajib, A. J., Birrer, S., et al. 2023, arXiv e-prints, arXiv:2311.09307, doi: [10.48550/arXiv.2311.09307](https://doi.org/10.48550/arXiv.2311.09307)
- Tessore, N., Bellagamba, F., & Metcalf, R. B. 2016, *MNRAS*, 463, 3115, doi: [10.1093/mnras/stw2212](https://doi.org/10.1093/mnras/stw2212)
- Thomas, J., Saglia, R. P., Bender, R., et al. 2007, *MNRAS*, 382, 657, doi: [10.1111/j.1365-2966.2007.12434.x](https://doi.org/10.1111/j.1365-2966.2007.12434.x)
- Tortora, C., Hunt, L. K., & Ginolfi, M. 2022, *A&A*, 657, A19, doi: [10.1051/0004-6361/202140414](https://doi.org/10.1051/0004-6361/202140414)
- Tortora, C., La Barbera, F., Napolitano, N. R., et al. 2014, *MNRAS*, 445, 115, doi: [10.1093/mnras/stu1616](https://doi.org/10.1093/mnras/stu1616)
- Tortora, C., La Barbera, F., Napolitano, N. R., et al. 2016, in *Astrophysics and Space Science Proceedings*, Vol. 42, The Universe of Digital Sky Surveys, ed. N. R. Napolitano, G. Longo, M. Marconi, M. Paolillo, & E. Iodice, 215, doi: [10.1007/978-3-319-19330-4_33](https://doi.org/10.1007/978-3-319-19330-4_33)
- Tortora, C., Napolitano, N. R., Romanowsky, A. J., & Jetzer, P. 2010, *ApJL*, 721, L1, doi: [10.1088/2041-8205/721/1/L1](https://doi.org/10.1088/2041-8205/721/1/L1)
- Tortora, C., Romanowsky, A. J., & Napolitano, N. R. 2013, *ApJ*, 765, 8, doi: [10.1088/0004-637X/765/1/8](https://doi.org/10.1088/0004-637X/765/1/8)
- Treu, T., Auger, M. W., Koopmans, L. V. E., et al. 2010, *ApJ*, 709, 1195, doi: [10.1088/0004-637X/709/2/1195](https://doi.org/10.1088/0004-637X/709/2/1195)
- Treu, T., Dutton, A. A., Auger, M. W., et al. 2011, *MNRAS*, 417, 1601, doi: [10.1111/j.1365-2966.2011.19378.x](https://doi.org/10.1111/j.1365-2966.2011.19378.x)
- Treu, T., Koopmans, L. V., Bolton, A. S., Burles, S., & Moustakas, L. A. 2006, *ApJ*, 640, 662, doi: [10.1086/500124](https://doi.org/10.1086/500124)
- Treu, T., & Koopmans, L. V. E. 2002, *ApJ*, 575, 87, doi: [10.1086/341216](https://doi.org/10.1086/341216)
- . 2004, *ApJ*, 611, 739, doi: [10.1086/422245](https://doi.org/10.1086/422245)
- van Dokkum, P., Brammer, G., Wang, B., Leja, J., & Conroy, C. 2024, *Nature Astronomy*, 8, 119, doi: [10.1038/s41550-023-02103-9](https://doi.org/10.1038/s41550-023-02103-9)
- Wang, C., Li, R., Zhu, K., et al. 2024, *MNRAS*, 527, 1580, doi: [10.1093/mnras/stad3214](https://doi.org/10.1093/mnras/stad3214)
- Wang, Y., Vogelsberger, M., Xu, D., et al. 2019, *MNRAS*, 490, 5722, doi: [10.1093/mnras/stz2907](https://doi.org/10.1093/mnras/stz2907)
- Weidner, C., Ferreras, I., Vazdekis, A., & La Barbera, F. 2013, *MNRAS*, 435, 2274, doi: [10.1093/mnras/stt1445](https://doi.org/10.1093/mnras/stt1445)
- Wong, K. C., Tran, K.-V. H., Suyu, S. H., et al. 2014, *ApJL*, 789, L31, doi: [10.1088/2041-8205/789/2/L31](https://doi.org/10.1088/2041-8205/789/2/L31)
- Wright, A. H., Kuijken, K., Hildebrandt, H., et al. 2024, *A&A*, 686, A170, doi: [10.1051/0004-6361/202346730](https://doi.org/10.1051/0004-6361/202346730)
- Xu, D., Springel, V., Sluse, D., et al. 2017, *MNRAS*, 469, 1824, doi: [10.1093/mnras/stx899](https://doi.org/10.1093/mnras/stx899)
- Zhan, H. 2018, in *42nd COSPAR Scientific Assembly*, Vol. 42, E1.16–4–18
- Zhu, K., Lu, S., Cappellari, M., et al. 2023, *MNRAS*, 522, 6326, doi: [10.1093/mnras/stad1299](https://doi.org/10.1093/mnras/stad1299)
- . 2024, *MNRAS*, 527, 706, doi: [10.1093/mnras/stad3213](https://doi.org/10.1093/mnras/stad3213)

APPENDIX

A. MULTI-BAND LENS MODEL

In this appendix, we present the details of the multi-band lens modeling that we performed to obtain the source-uncontaminated photometry of the lens in 8 bands: $grZYJHK_s$. We used the same code LENSED and method as described in Section 2.2, but applied them to the KiDS and VIKING images instead of the AO image. We modeled the lens light, source light and mass distribution with de Vaucouleur profile, elliptical Sérsic profile, and SIE profile, respectively. We varied the parameters of these profiles independently in each band, except for the following cases: we fixed the effective radius and the axis ratio of the foreground light, as well as the Sérsic index and the axis ratio of the source light in the NIR bands, to the value obtained from the AO image, since the resolution in this bands is very low in these bands. We used the same MCMC inference as in Section 2.2 to explore the parameter space and obtain the best-fitting models and the uncertainties.

Table A1 summarizes the main parameters obtained from the multi-band lens modeling. The total magnitudes of the lens, as well as the effective radii, the axis ratios, and the position angles, are reported in the table. The Einstein radii, axis ratios, and position angles of the mass profiles are also shown. Fig. 3 shows the images, the models, and the residuals in each band. The models can reproduce the observed features of the lens system, such as the lensed arcs and the counter-image, with small residuals. The parameters obtained from the multi-band lens modeling are consistent with those obtained from the AO model within the uncertainties. Despite leaving the total mass parameters of the lens model free to vary, we have found an incredibly tight distribution of their values over the 8-band models, with the $R_{\text{Ein}} = 1.28 \pm 0.02$ arcsec, the $q = 0.94 \pm 0.02$ and the $\text{PA} = 148 \pm 9$ deg, which are fully consistent with the AO parameters in Tab. 1. This indicating that the mass distribution of the lens is robust and stable. The effective radii of the light of the central galaxy show some variation between the gr bands and the other bands, which is mainly due to the low signal-to-noise ratio in the gr bands.

Table A1. Parameters of the multi-band lens model.

band	g	r	i	Z	Y	J	H	Ks
mag	23.82	22.75	22.13	21.24	20.68	20.24	19.74	19.13
R_{eff} (arcsec)	1.76	1.57	0.48	0.26	0.26	0.26	0.26	0.26
q_*	0.52	0.80	0.6411	0.85	0.85	0.85	0.85	0.85
PA_* (deg)	78.59	84.02	80.59	85.57	48.66	144.75	76.47	170.88
R_{Ein} (arcsec)	1.31	1.30	1.28	1.28	1.29	1.30	1.27	1.23
q_{mass}	0.94	0.95	0.94	0.95	0.92	0.90	0.95	0.97
PA_{mass} (deg)	148.51	145.52	154.48	140.82	159.13	132.26	142.28	157.89

NOTE. —Parameters of the multi-band lens modelling. From top to bottom, we show the magnitudes, effective radius, position angle of the deflector light, and the Einstein radius, axis ratio, and position angle of the mass distribution, for the multiple band lens modeling.